Intermetallics 54 (2014) 148–153

Contents lists available at ScienceDirect

Intermetallics

journal homepage: www.elsevier.com/locate/intermet

On the entropic stabilisation of an $Al_{0.5}CrFeCoNiCu$ high entropy alloy

N.G. Jones*, J.W. Aveson, A. Bhowmik, B.D. Conduit, H.J. Stone

Department of Materials Science and Metallurgy, University of Cambridge, 27 Charles Babbage Road, Cambridge CB3 0FS, UK

ARTICLE INFO

Article history:
Received 21 March 2014
Received in revised form
9 June 2014
Accepted 12 June 2014
Available online

Keywords:
A. High–entropy alloys
B. Phase stability
B. Thermodynamic properties

ABSTRACT

The extent to which configurational entropy can stabilise a single solid solution in an $Al_{0.5}CrFeCoNiCu$ high entropy alloy has been assessed through characteristion of samples following casting and heat treatment at 1000 °C. At temperatures between 1000 °C and the onset of melting, the alloy was shown to be within a two phase field and these phases were stable following prolonged exposure at elevated temperature. X-ray and transmission electron diffraction indicated that both constituent phases had an *fcc* structure. Therefore, these phases share a Gibbs energy curve that must contain two local minima at the solidus temperature, rather than the single minimum required for a continuous solid solution. These observations indicate that there is no temperature at which this material is in a stable, solid state single phase field and that therefore, the configurational complexity is insufficient to stabilise a solid solution phase against enthalpic effects.

1. Introduction

High entropy alloys (HEAs) are a relatively new class of metallic materials that have no primary element, but are instead based on approximately equiatomic additions of five or more individual elements [1,2]. Traditionally, such mixtures would be expected to contain multiple intermetallic phases. However, X-ray and electron diffraction data from these materials has often revealed only a limited number of simple crystal structures, such as *fcc* or *bcc* and their related superlattice structures. It has been suggested that the apparent stability of these phases results from a high configurational entropy that outweighs the enthalpy of formation of intermetallic phases [2].

AlCrFeCoNiCu was one of the first reported high entropy alloys and initial work indicated that, with Al ratios less than 0.65, the as-cast microstructure contained only a single *fcc* phase. Higher Al contents promoted the formation of a *bcc* based phase [2]. Since then, a phase diagram for the system has been proposed, in which $Al_{0.5}CrFeCoNiCu$ was reported to have two solid state phase fields; *fcc* + *fcc* at temperatures above 700 °C and $L1_2$ + *fcc* below 700 °C [3]. More recent studies of the same alloy have suggested there is equilibrium between two *fcc* phases and an *ordered fcc* phase at temperatures immediately below the solidus [4] and that precipitation of additional intermetallic phases occurs at intermediate temperatures [4,5]. These observations are in direct contrast to the phase equilibria proposed in Ref. [3]. Complementary thermodynamic predictions suggested that these intermetallic phases should indeed form. However, whilst broadly similar, none of the predicted phase assemblies in Ref. [4] match those found experimentally. This disparity is perhaps unsurprising as the compositions considered are well outside the assessed compositional space of the underlying databases.

Several studies on other high entropy alloys have reported that their solid solutions are stable with respect to heat treatment, albeit segregation has been observed to form other entropically stabilised phases [6–9]. Interestingly, there have also been reports of microstructural evolution through both age hardening [5,10–12] and precipitation [5,12–15] following exposure at elevated temperatures. These contrasting results illustrate the complexity of the phase equilibria in this class of alloys and the need to determine phase stability on a system by system basis. This need is further highlighted by a recent study that considered phase stability by systematically replacing each element in an equiatomic, five component alloy [16]. Whilst the base alloy formed a single solid solution, the microstructures of all the substitutional variants contained intermetallic phases, indicating that configurational entropy was not dominating the phase equilibria.

Despite the lack of agreement surrounding the phase stability of these materials, their reported mechanical and environmental properties are promising, both at ambient and elevated temperatures, leading to significant interest in their use for a wide range of applications [1–3,17–19]. However, resolving the uncertainty of the

* Corresponding author. Tel.: +44 1223 334367.
E-mail address: ngj22@cam.ac.uk (N.G. Jones).

http://dx.doi.org/10.1016/j.intermet.2014.06.004

phase stability of these materials is critical for their future selection, manufacture and exploitation. Therefore, in this study, the phase stability of $Al_{0.5}$CrFeCoNiCu has been studied following long term heat treatment directly from the as-cast state. The results obtained contradict all the previously proposed phase equilibria of this alloy and demonstrate, for the first time, that a solid state single phase field does not exist at any temperature.

2. Experimental

A 40 g ingot of $Al_{0.5}$CrFeCoNiCu was prepared via arc melting in an inert atmosphere from elemental metals with purity ≥99.95%. To achieve homogeneity, the ingot was inverted and remelted five times. A short section, ~10 mm long, was cut from the as-cast ingot, encapsulated in an evacuated, argon backfilled quartz ampoule and heat treated for 1000 h at 1000 °C, followed by an immediate water quench. Microstructural characterisation was carried out using backscattered electron imaging (BSEI) in a JEOL 5800 Scanning Electron Microscope. Compositional data was obtained in the same microscope using an Oxford Instruments energy dispersive X-ray (EDX) spectroscopy system. Individual phase compositions were determined by averaging five point analyses, and the bulk composition assessed from five, large area (~500 × 500 μm) scans. The bulk analyses indicated that each of the elemental components was within 1 at% of the nominal concentration. Higher magnification images of ion milled thin foils were acquired using a JEOL 200CX Transmission Electron Microscope (TEM) and selected area diffraction patterns (SADP) taken from different regions of interest. Macroscopic crystallographic information was obtained via X-ray diffraction using a Philips PW1050 diffractometer in Bragg–Brentano geometry with CuKα radiation, a 0.64 mm divergence slit, a 0.2 mm receiving slit and 0.04° steps in 2θ with 20 s count times. Differential Scanning Calorimetry (DSC) was performed between room temperature and 1400 °C under flowing argon using a Netzsch 404 high temperature calorimeter at a heating rate of 10 °C min^{-1}.

3. Results

The as-cast material, Fig. 1a, exhibited a dendritic microstructure with Fe, Co, Cr rich dendrites and Cu, Al rich interdendritic material. EDX determined phase compositions are given in Table 1. Casting-induced porosity was also observed in the interdendritic regions. X-ray diffraction from this material, Fig. 1b, revealed peaks corresponding to an *fcc* structure, consistent with previous reports [2]. In addition, several low intensity peaks were also present in the spectra, as identified by diamond markers, indicating that a small volume fraction of at least one other structure existed within the material in this condition. However, the area of these smaller peaks was inconsistent with the volume fraction of interdendritic material observed in Fig. 1a.

Closer examination of the *fcc* peaks revealed a distinct shouldering on the low 2θ side. The observation of two phases in the microstructure, Fig. 1a, and the absence of diffraction peaks of sufficient intensity to account for the second phase suggested that both phases had the *fcc* structure and that the distinct shouldering arose as a result of the difference in the lattice parameters of these two phases, rather than solidification-induced microsegregation of the dendrites. To account for this, each diffraction peak was fitted with two profile functions using a Levenberg–Marquandt non-linear least squares algorithm in Wavemetrics Igor Pro. Each profile function was a summation of two Gaussian peaks, accounting for the contributions from CuKα_1 and CuKα_2 radiation. The relative position, intensity and width of the CuKα_1 and CuKα_2 peaks were constrained, in line with diffraction theory, such that each profile function had only three fitting variables. An example of fitted data is shown in the inset of Fig. 1b, along with the two constituent profile functions. The lattice parameters of the two phases were evaluated from the fitted Bragg angles of all *fcc* reflections through a non-linear least squares minimisation and were determined to be 3.595 and 3.602 Å respectively.

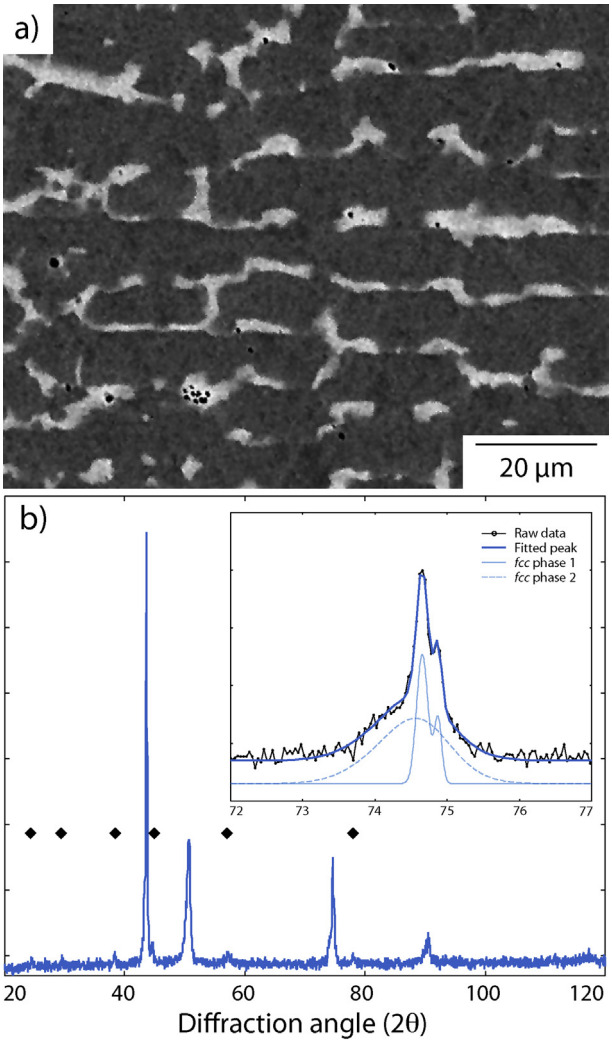

Fig. 1. As-cast $Al_{0.5}$CrFeCoNiCu; a) BSEI showing the two phase dendritic microstructure, and b) corresponding X-ray diffraction spectrum indicating an *fcc* structure, the diamond markers highlight the presence of another phase, and inset showing the fitted {220} peak, illustrating that both dendritic and interdendritic phases are *fcc*.

The microstructure observed following heat treatment for 1000 h at 1000 °C, Fig. 2a, was similar to that of the as-cast material, in agreement with the observations in Ref. [4]. However, in contrast to the as-cast material, the interfaces between the two phases were

Table 1
Summary of phase compositions (in at%) determined from five individual spot EDX analyses, the standard deviation of each measurement is less than 1%.

Condition	Phase	Al	Cr	Fe	Co	Ni	Cu
As-cast	Dendritic (grey)	6	23	23	21	18	9
	Interdendritic (white)	12	7	7	7	16	51
1000 °C 1000 h	Dendritic (grey)	7	23	23	20	19	8
	Interdendritic (white)	11	4	5	5	16	59

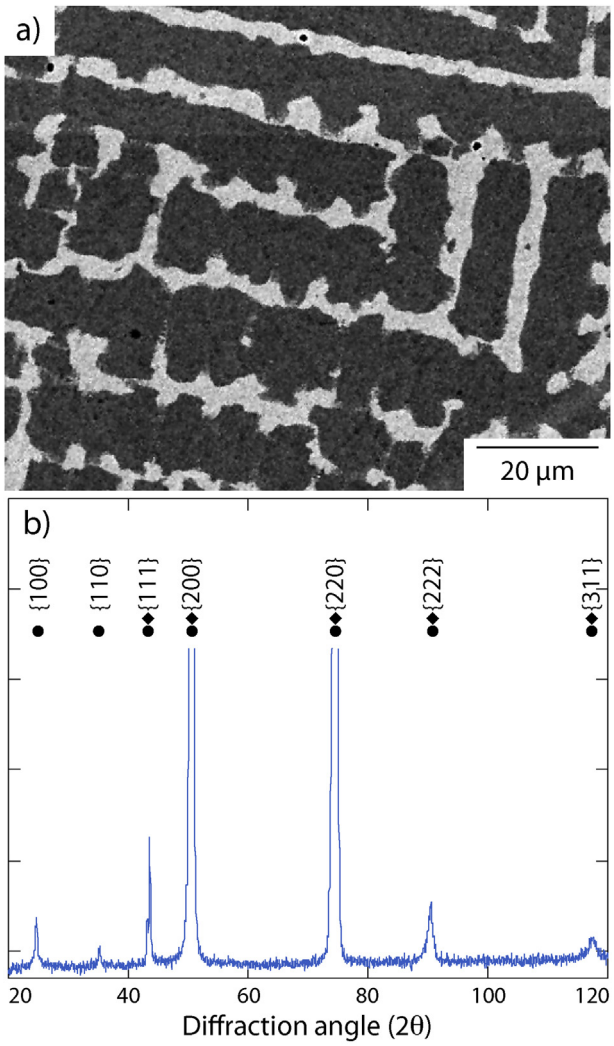

Fig. 2. $Al_{0.5}CrFeCoNiCu$ heat treated for 1000 h at 1000 °C; a) BSEI showing a two phase dendritic microstructure, similar to that of the as-cast, and b) the corresponding X-ray diffraction spectrum showing the presence of $L1_2$ superlattice reflections in addition to those of two *fcc* phases.

sharper, suggesting homogenisation had occurred during thermal exposure. Indeed, evidence of this was observed in the phase compositions given in Table 1, which indicated small variations in the elemental partitioning between the two phases in the as-cast and heat treated states.

The corresponding X-ray diffraction spectrum of the annealed sample, Fig. 2b, showed two sets of overlapping *fcc* reflections, similar to Fig. 1b, with average lattice parameters of 3.597 and 3.632 Å. The similarity between this diffraction pattern and that obtained from the as-cast sample supports the assertion that the shouldering in the as-cast state arose as a result of two overlayed *fcc* diffraction patterns, rather than as a result of any microsegregation. However, following annealing, the intensity and definition of the low angle peaks were significantly enhanced and could be indexed with the $L1_2$ structure. Detailed investigation into the source of these reflections was conducted using transmission electron microscopy, Fig. 3 and Fig. 4, as a complete *fcc* → $L1_2$ ordering transformation has previously been suggested [3]. A bright field image of a dendrite interface is shown in Fig. 3a, with the interdendritic and dendritic material labelled as regions B and C respectively. The SADP from the interdendritic material, Fig. 3b, showed reflections corresponding to an *fcc* structure, whilst the SADP from the dendrites, Fig. 3c, showed diffraction spots consistent with the presence of an $L1_2$ superlattice structure. Dark field imaging from a superlattice reflection, Fig. 4, showed that the $L1_2$ phase formed as small, ~25 nm, cuboidal precipitates within the *fcc* matrix, akin to gamma prime in Ni-base superalloys.

DSC thermograms measured during the heating and remelting of as-cast and annealed material are shown in Fig. 5. Both traces show a pronounced, sigmoidal deviation at ~850 °C, which was sharper in the annealed material, and two large, endothermic events at ~1150 and ~1350 °C.

Sigmoidal deviations are commonly observed in the thermograms of Ni-base superalloys and correspond to the gamma prime solvus temperature [20]. As fine $L1_2$ precipitates were observed in the *fcc* dendrites, the deviation at ~850 °C can be attributed to the dissolution of this phase. The occurrence of the sigmoidal feature in both thermograms suggests that the $L1_2$ precipitates were also present in the as-cast microstructure, and this structure accounted for the majority of the low intensity peaks in Fig. 1b. The wider temperature range over which the $L1_2$ dissolves in the as-cast sample may be attributed to compositional variations across cored dendrites and the corresponding changes in the $L1_2$ solvus temperature. The smaller endothermic peak at ~1150 °C is typical of the incipient melting of an interdendritic constituent, whilst the larger peak at ~1350 °C is consistent with the bulk melting of a

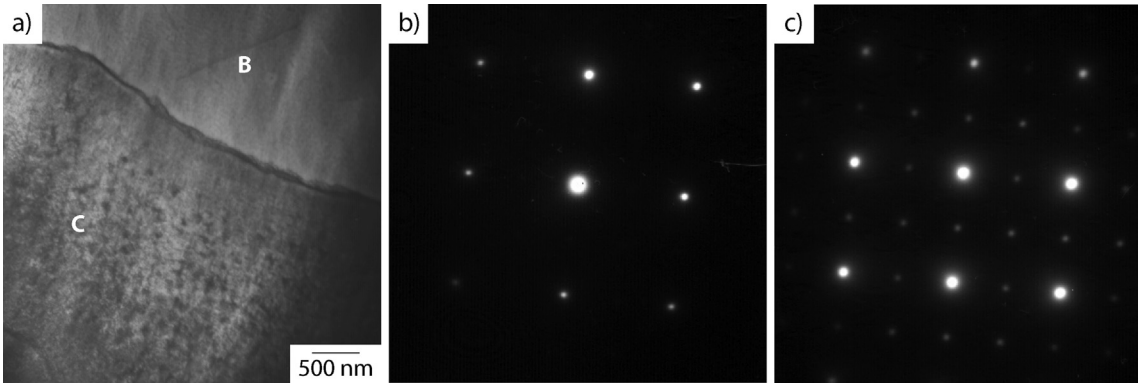

Fig. 3. a) Bright field TEM micrograph of a dendrite interface in $Al_{0.5}CrFeCoNiCu$ following 1000 h heat treatment at 1000 °C, b) [100] zone axis SADP from the interdendritic region (B) indicating an *fcc* structure, and c) [100] zone axis SADP from the within the dendrite (C) showing the presence of superlattice reflections consistent with the presence of $L1_2$ precipitates.

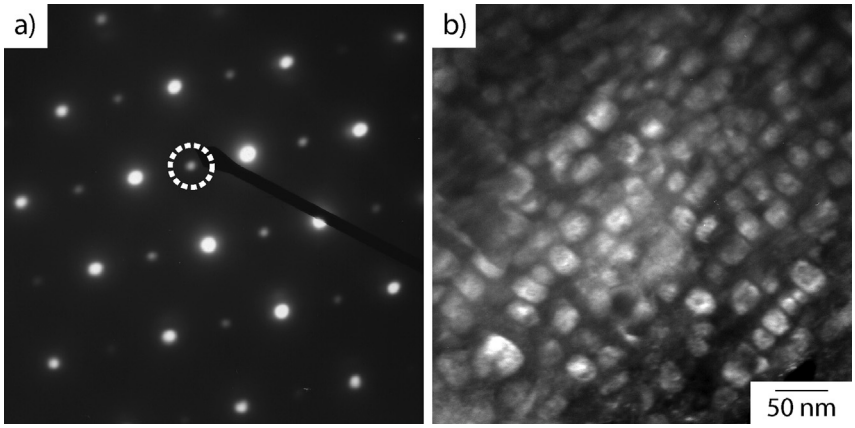

Fig. 4. a) [110] zone axis SADP from within a dendrite, indicating the superlattice reflection used to form the dark field image, and b) dark field image showing the cuboidal morphology of the $L1_2$ precipitates.

compositionally graded dendrite. These two melting temperatures are in good agreement with those reported in Ref. [3]. In addition, small deviations can be seen above 1000 °C in both thermograms. However, no microstructural feature has been identified that may account for these deviations.

4. Discussion

Metastable solidification phases would decompose during long duration thermal exposures and evidence of that transformation would be seen in both the differential thermal analysis and the corresponding microstructures. The consistency between the microstructures, phase compositions and thermograms of the as-cast and 1000 °C annealed samples indicates that the solidification phases are not simply a result of solute segregation and kinetic limitations. Further, no phase transformations were observed between 1000 °C and the onset of melting in the thermograms, nor was there any evidence of phase evolution between Figs. 1 and 2, beyond the elimination of solidification induced microsegregation. Therefore, it can be concluded that the two phases formed during solidification are thermodynamically stable above 1000 °C. This conclusion is in agreement with the predictions of Tong et al. [3] and in contrast to the results of Ng et al. [4], who suggested two *fcc* phases and an *ordered fcc* phase were stable immediately below the solidus temperature. The differential thermal analysis data, Fig. 5, suggests that the $L1_2$ phase precipitated on cooling through a solvus at ~850 °C, rather than being present at higher temperatures. This interpretation is also consistent with the fine scale of the $L1_2$ precipitates observed in Fig. 4. If these precipitates had been present during the extended annealing treatment, then significant coarsening would have occurred. Conversely, fine scale particles, such as those observed here, would be expected if the solid state transformation occurred during cooling, where nucleation rates would be high and growth limited. Such behaviour is consistent with the metallurgy of Ni-base superalloys, where the solid state precipitation of the gamma prime phase occurs even at extremely high cooling rates and may lead to gamma prime precipitates of similar size and morphology to those seen here [21–26].

Based on these observations, a summary of the transformation pathway of $Al_{0.5}CrFeCoNiCu$ when rapidly cooled from a liquid state is given below. This pathway differs to those proposed in Refs. [3] and [4], with the $L1_2$ phase precipitating within fcc_1 during cooling, rather than forming by complete ordering of fcc_1 [3],[1] or as a solidification product [4].

$$l \rightarrow l + fcc_1 \rightarrow fcc_1 + fcc_2 \rightarrow (fcc_1 + L1_2) + fcc_2$$

The evidence gathered in this study indicates that, at temperatures above 1000 °C, $Al_{0.5}CrFeCoNiCu$ is in a two phase field in which both constituent phases have an identical crystal structure and similar lattice parameters. Whilst this has been previously identified [3], its significance to the thermodynamics of this alloy and the concept of entropic stabilisation, has not been discussed.

Classical thermodynamics states that for two components to exhibit complete solid solubility in each other they must be extremely similar in terms of atomic size, electronic configuration and must crystallise in the same structure [27,28]. The Gibbs energy curve that describes this behaviour has a single minimum and is strongly dependent on the entropy of mixing. A similar Gibbs energy curve, with a single minimum, would be expected in multicomponent alloys if, as suggested in Ref. [2], the configurational complexity of the alloy enabled the entropic term to dominate the

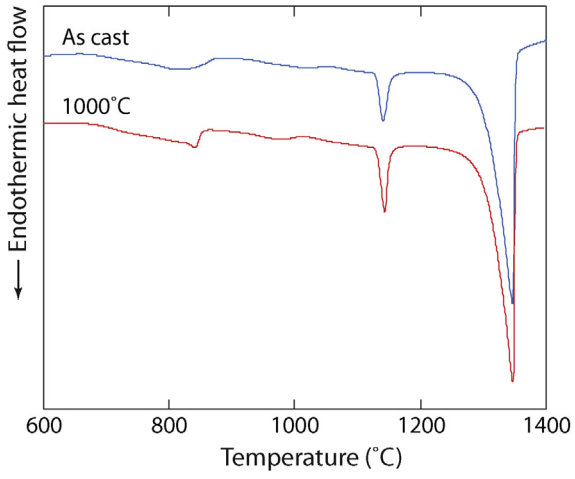

Fig. 5. DSC thermogram of $Al_{0.5}CrFeCoNiCu$ during heating and remelting from the as-cast and 1000 °C annealed conditions.

[1] It should be noted that $L1_2$ precipitation in fcc_1 is reported in the text of reference [3]. However, the proposed phase diagram in the same work indicated an ordering transformation.

enthalpic term. However, the present work has shown that between 1000 °C and the solidus temperature, $Al_{0.5}$CrFeCoNiCu exists as two *fcc* structures, which cannot be described by a Gibbs energy curve of this form.

The Gibbs energy curve for any given crystal structure extends continuously across compositional space. Therefore, two phases that have the same crystal structure must also have a common Gibbs energy curve. In addition to the case of complete solubility described above, as temperature decreases, the enthalphic term can begin to dominate the entropic term, leading to the Gibbs energy curve developing two local minima [27–29]. This leads to partial solubility between the two elements and the occurrence of a miscibility gap between the two solid solutions. If the Gibbs energy curve develops two minima above the solidus temperature, then the phase diagram will be either eutectic or peritectic, for example, the Cu–Ag [30] or Pt–Ag [31] binary systems respectively. In contrast, if the Gibbs energy curve develops two minima below the solidus temperature, then a continuous solid state single phase field will exist at higher temperatures, giving way to a miscibility gap and phase separation at lower temperatures, for example the Au–Ni system [32]. These principles also apply in higher order systems, and the necessity for continuous Gibbs energy curves is elegantly demonstrated by considering the Cu–Ag–Au ternary system. The *fcc* Cu and *fcc* Ag phases in the Cu–Ag binary system show only limited solubility in each other, with no continuous solid state single phase field across the composition range. However, complete solid solubility, and a single *fcc* phase field, can be achieved by sufficient additions of Au, for instance, concentrations greater than 30 at% at 750 °C [33]. This situation cannot be described unless the Gibbs energy curve is continuous across the entire ternary composition space.

The observation that $Al_{0.5}$CrFeCoNiCu solidified as two compositionally distinct *fcc* structures, rather than a cored single phase of continuously varying composition, requires the corresponding Gibbs energy curve to contain two local minima at the temperature at which the final stage of solidification occurred. Microstructural examination has shown that these two phases are stable with respect to prolonged aging at both 1000 °C in the present work and at 1100 °C in Refs. [4], indicating the existence of a two phase equilibrium phase field in this temperature range. Thus, if an entropically stabilised single solid solution phase was to exist, it could only do so between 1100 °C and the onset of melting at 1150 °C. No evidence of a transformation was observed in the DSC thermograms between these temperatures and as the extent of entropic stabilisation will decrease at lower temperatures, it can be concluded that there is no a single solid solution phase field in this material. Furthermore, the elemental partitioning associated with the formation of the two phases will significantly reduce their entropic stability, increasing their susceptibility to further phase decomposition.

5. Conclusions

The phase stability of an $Al_{0.5}$CrFeCoNiCu alloy has been assessed following casting and 1000 h heat treatment at 1000 °C. The alloy solidified as two compositionally distinct *fcc* phases, which were observed to be stable following heat treatment at 1000 °C. An $L1_2$ phase was also present in the as-cast and 1000 °C annealed microstructures. However, in contradiction to previous reports, this phase was shown to precipitate during cooling and had a solvus temperature of ~850 °C. The two *fcc* structures are therefore the thermodyanimcally stable equilibrium phases at high temperature and, as they possess the same crystal structure, share a Gibbs energy curve. Correspondingly, this Gibbs energy curve must contain two local minima, as opposed to one for a continuous solid solution. Therefore, enthalpic terms dominate the behaviour of this alloy and a single, stable, solid state phase field does not exist in this material.

Acknowledgements

The authors would like acknowledge K.A. Roberts, K.A. Christofidou and A. J. Knowles for their assistance, W.J. Clegg for his insightful comments, and the EPSRC/Rolls-Royce Strategic Partnership for funding (NGJ, AB and HJS under EP/H500375/1, JWA and BDC under EP/H022309/1).

References

[1] Yeh J. High-entropy multielement alloys. US Patent App. 10/133,495; 2002.
[2] Yeh J, Chen S, Lin S, Gan J, Chin T, Shun T, et al. Nanostructured high-entropy alloys with multiple principal elements: novel alloy design concepts and outcomes. Adv Eng Mater 2004;6:299–303.
[3] Tong C, Chen Y, Chen S, Yeh J, Shun T, Tsau C, et al. Microstructure characterization of Al_xCoCrCuFeNi high-entropy alloy system with multiprincipal elements. Metallurgical Mater Trans A-Physical Metallurgy Mater Sci 2005;36A:881–93.
[4] Ng C, Guo S, Luan J, Shi S, Liu CT. Entropy-driven phase stability and slow diffusion kinetics in an $Al_{0.5}$CoCrCuFeNi high entropy alloy. Intermetallics 2012;31:165–72.
[5] Tsai C-W, Tsai M-H, Yeh J-W, Yang CC. Effect of temperature on mechanical properties of $Al_{0.5}$CoCrCuFeNi wrought alloy. J Alloys Compd 2010;490:160–5.
[6] Senkov ON, Wilks GB, Miracle DB, Chuang CP, Liaw PK. Refractory high-entropy alloys. Intermetallics 2010;18:1758–65.
[7] Lin C-M, Tsai H-L, Bor H-Y. Effect of aging treatment on microstructure and properties of high-entropy $Cu_{0.5}$CoCrFeNi alloy. Intermetallics 2010;18:1244–50.
[8] Wen LH, Kou HC, Li JS, Chang H, Xue XY, Zhou L. Effect of aging temperature on microstructure and properties of AlCoCrCuFeNi high-entropy alloy. Intermetallics 2009;17:266–9.
[9] Lin C-M, Tsai H-L. Effect of annealing treatment on microstructure and properties of high-entropy FeCoNiCr$Cu_{0.5}$ alloy. Mater Chem Phys 2011;128:50–6.
[10] Shun T-T, Hung C-H, Lee C-F. Formation of ordered/disordered nanoparticles in FCC high entropy alloys. J Alloys Compd 2010;493:105–9.
[11] Shun T-T, Du Y-C. Age hardening of the $Al_{0.3}$CoCrFeNi$C_{0.1}$ high entropy alloy. J Alloys Compd 2009;478:269–72.
[12] Chen S-T, Tang W-Y, Kuo Y-F, Chen S-Y, Tsau C-H, Shun T-T, et al. Microstructure and properties of age-hardenable Al_xCr$Fe_{1.5}$Mn$Ni_{0.5}$ alloys. Mater Sci Eng A 2010;527:5818–25.
[13] Lin C-M, Tsai H-L. Evolution of microstructure, hardness, and corrosion properties of high-entropy $Al_{0.5}$CoCrFeNi alloy. Intermetallics 2011;19:288–94.
[14] Shun T-T, Du Y-C. Microstructure and tensile behaviors of FCC $Al_{0.3}$CoCrFeNi high entropy alloy. J Alloys Compd 2009;479:157–60.
[15] Lin C-M, Tsai H-L. Equilibrium phase of high-entropy FeCoNiCr$Cu_{0.5}$ alloy at elevated temperature. J Alloys Compd 2010;489:30–5.
[16] Otto F, Yang Y, Bei H, George EP. Relative effects of enthalpy and entropy on the phase stability of equiatomic high-entropy alloys. Acta Mater 2013;61:2628–38.
[17] Chen Y, Duval T, Hung U, Yeh J, Shih H. Microstructure and electrochemical properties of high entropy alloys – a comparison with type-304 stainless steel. Corros Sci 2005;47:2257–79.
[18] Chen Y, Hong U, Shih H, Yeh J, Duval T. Electrochemical kinetics of the high entropy alloys in aqueous environments – a comparison with type 304 stainless steel. Corros Sci 2005;47:2679–99.
[19] Hsu Y, Chiang W, Wu J. Corrosion behavior of FeCoNiCrCu_x high-entropy alloys in 3.5% sodium chloride solution. Mater Chem Phys 2005;92:112–7.
[20] Sponseller DL. Differential thermal analysis of nickel-base superalloys. Superalloys 1996;1996:259–70.
[21] Babu SS, Miller MK, Vitek JM, David SA. Characterization of the microstructure evolution in a nickel base superalloy during continuous cooling conditions. Acta Mater 2001;49:4149–60.
[22] Furrer DU, Fecht H-J. γ' formation in superalloy U720Li. Scr Mater 1999;40:1215–20.
[23] Yoon KE, Noebe RD, Seidman DN. Effects of rhenium addition on the temporal evolution of the nanostructure and chemistry of a model Ni–Cr–Al superalloy. I: experimental observations. Acta Mater 2007;55:1145–57.
[24] Van Der Molen EH, Oblak JM, Kriege OH. Control of γ' particle size and volume fraction in the high temperature superalloy Udimet 700. Metall Trans A 1971;2:1627–33.
[25] Collins DM, Yan L, Marquis EA, Connor LD, Ciardiello JJ, Evans AD, et al. Lattice misfit during ageing of a polycrystalline nickel-base superalloy. Acta Mater 2013;61:7791–804.

[26] Kissinger RD. Cooling path dependent behavior of a supersolvus heat treated nickel base superalloy. Superalloys 1996;1996:687–95.
[27] Cottrell AH. Theoretical structural metallurgy. 2 ed. London: Edward Arnold; 1960.
[28] Hume-Rothery W, Smallman RE, Haworth CW. The structure of metals and alloys. 5th ed. The Institute of Metals; 1969.
[29] Swalin RA. Thermodynamics of solids. Wiley; 1972.
[30] Murray JL. Calculations of stable and metastable equilibrium diagrams of the Ag–Cu and Cd–Zn systems. Metallurgical Mater Trans A 1984;15:261–8.
[31] Okamoto H. Ag–Pt. J Phase Equilibria 1997;18:485.
[32] Okamoto H, Massalski TB. Au–Ni. In: Massalski TB, editor. Binary alloy phase diagrams, ASM; 1990. pp. 402–4.
[33] Prince A, Liang P. Ag–Au–Cu. In: Ternary alloys. VCH; 1995.